Maxwell equation simulations of coherent optical photon emission from shock waves in crystals

Evan J. Reed,[1,2,*] Marin Soljačić,[1] and J. D. Joannopoulos[1]
[1]*Center for Materials Science and Engineering and Research Laboratory of Electronics, Massachusetts Institute of Technology, Cambridge, Massachusetts 02139, USA*
[2]*Lawrence Livermore National Laboratory, Livermore, California 94551, USA*
(Received 29 November 2006; published 18 May 2007)

We have predicted that weak coherent radiation in the 1–100 THz frequency regime can be emitted under some circumstances when a shock wave propagates through a polarizable crystal, like NaCl [Reed *et al.*, Phys. Rev. Lett. **96**, 013904 (2006)]. In this work, we present and analyze a new model of a shocked polarizable crystal that is amenable to systematic analytical study and direct numerical solution of Maxwell's equations to predict emitted coherent field amplitudes and properties. Our simulations and analysis indicate that the field amplitude of the effect decreases rapidly with increasing shock front rise distance. These models establish a fundamental limit of the ratio of emitted terahertz amplitude to the static polarization of a material. While this effect is treated classically in our previous work, we present a quantum perturbation analysis showing that it can also occur in the low-amplitude emission quantum limit.

DOI: 10.1103/PhysRevE.75.056611 PACS number(s): 41.20.−q, 41.90.+e, 42.50.Gy

I. INTRODUCTION

In our previous work, we predicted that weak coherent radiation in the 1–100 THz frequency regime can be emitted under some circumstances when a shock wave propagates through a polarizable crystal, like NaCl [1]. The coherence of the emitted radiation comes from the spatial coherence of the crystalline lattice and the constant propagation speed of the shock wave. We believe the mechanism responsible for this type of emission is fundamentally distinct from existing sources of coherent optical radiation.

In our original work and in a related paper [1,2], we studied this effect by performing molecular dynamics simulations of shock waves in NaCl crystals. While these simulations provide an accurate description of the phenomenon, they are not amenable to systematic study of the phenomenon with respect to changes in the key parameters like the shock front rise time and static dielectric properties. The molecular dynamics simulations also do not solve Maxwell's equations directly.

Throughout this work, we utilize a classical one-dimensional (1D) model of a shock wave propagating through a polarizable crystal in order to study the coherent emission phenomenon. We use a finite-difference time-domain (FDTD) technique [9] to solve the coupled equations for the polarizable crystal and the electric and magnetic fields. The model is used to study the variation of coherent emission properties with shock front thickness and dielectric properties of the crystal. We also develop some simple analytical models of the shocked crystal to characterize the emission amplitude dependence on the shock front thickness and dielectric properties. These models establish a fundamental limit of the ratio of emitted terahertz (THz) amplitude to the static polarization of a material. Finally, we present a quantum perturbation analysis showing that coherently related photons are emitted even in the quantum case of very low-amplitude emission.

*Electronic address: reed23@llnl.gov

II. ANALYTICAL THEORY

It is well known that shock waves can induce static polarizations in a variety of materials. This phenomenon was first experimentally observed in the 1960s by measuring the time dependence of the current generated in a shocked material [3,4]. For some distance behind the planar shock front, materials are typically characterized by a state of increasing uniaxial stress, i.e., the spatial gradient in the shock propagation direction component of the stress is nonzero. Such a spatial stress gradient can lead to the creation of a static material polarization or a shift in the existing static polarization. The broken symmetry can potentially lead to a static electric polarization along the shock propagation direction in any material, including isotropic liquids like water [5].

In this work, we consider a special case of shock-induced polarization that occurs only in crystalline materials when the shock front becomes very sharp, i.e., the shock front rise distance is a few lattice planes of the crystal or less. In this case, the polarization current becomes temporally periodic since a current is produced each time the polarization of a single lattice unit shifts. Figure 1 illustrates this process in the limiting case where the shock front is one lattice unit in thickness. Each lattice unit of the crystal possesses a static polarization that is altered when the shock front passes over. In this case, the static polarization is perpendicular to the shock propagation direction. If the shock front propagates at a steady speed, the current generated during the shift in polarization of each lattice unit results in a temporally periodic polarization current at the shock front. The coherent polarization current can potentially yield coherent radiation at the same frequency. We have shown this effect can also occur in materials with no static polarization and when the polarization is parallel to the shock propagation direction [1,2].

Of key importance for this effect are a high degree of crystalline order and a crystal consisting of charged atoms or molecules that can couple to electromagnetic radiation, i.e., a polarizable crystal. In this work, we will show that the steepness of the shock front plays a crucial role in determining the

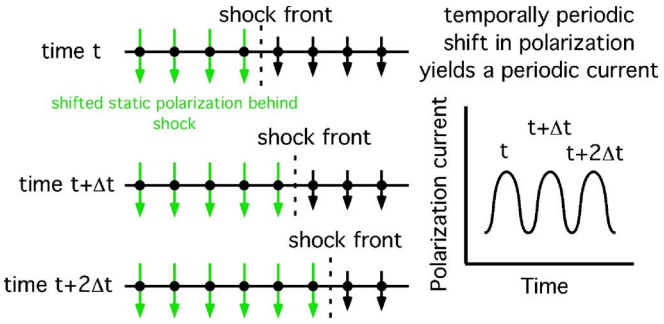

FIG. 1. (Color online) Schematic illustration of how a temporally periodic polarization current can be generated in the limiting case where the shock front is 1 lattice unit in thickness. Each lattice unit of the crystal possesses a static polarization that is altered in magnitude when the shock front passes over. If the shock front propagates at a steady speed, the current generated during the shift in polarization of each lattice unit results in a temporally periodic polarization current at the shock front.

amplitude of the periodic component of the polarization current. A shock front spread out over many lattice planes may yield smaller oscillations of the collective polarization and smaller oscillating polarization currents.

For typical ionic crystal lattice constants (0.1–1 nm) and typical shock speeds in these materials (1–10 km/s), the coherent oscillation frequencies lie in the range from 1 to 100 THz, i.e., the far infrared and slightly below into the THz frequency regime. Such frequencies are well above the highest frequencies detectable in shock polarization current measurement experiments, which utilize electronics to record signals. Optics-based techniques are typically used to detect signals in this frequency regime, rather than electronics-based techniques.

In this section we use analytical approaches to demonstrate the coherent nature of the emitted radiation and characterize the frequencies and amplitudes in terms of properties of the shock wave. To represent a 1D crystalline polarizable material, a polarizable element $P_n(t)$ that exists on each lattice point n located at $x=na$ obeys the equation

$$\frac{d^2P_n(t)}{dt^2} = \mu_n(t)E_n(t) - \Omega_n(t)^2P_n(t) - \bar{\Omega}_n(t)^2\bar{P} - \gamma\frac{dP_n(t)}{dt}. \tag{1}$$

Here, $\mu_n(t) \equiv (\alpha/V)\tilde{\Omega}_n(t)^2$, where α is the polarizability, V is the volume associated with each polarizable element, $\tilde{\Omega}_n(t)$ is a frequency containing the time dependence of $\mu_n(t)$, $\Omega_n(t)$ is the resonant frequency of the nth polarizable element, and γ is an absorption term. The term $\bar{\Omega}_n(t)^2\bar{P}$ gives rise to a ferroelectric polarization that can either be intrinsic to the material or generated using a static external electric field $E_{\text{external}}=-\bar{P}V/\alpha$. In general, a ferroelectric polarization or static external electric field is *not* required to observe the emission, as will be demonstrated later in this work, and has been demonstrated in our molecular dynamics simulations on NaCl with no static polarization. Ω_n is the local transverse optical mode frequency (ω_T) typically on the order of 10^{13} s^{-1} for phonons in ionic crystals. Equation (1) can model many polarizable materials when combined with Maxwell's equations in 1D,

$$-\frac{\partial B}{\partial x} = \frac{\partial E}{\partial ct} + 4\pi\frac{\partial P}{\partial ct}, \tag{2}$$

$$\frac{\partial E}{\partial x} = -\frac{\partial B}{\partial ct}. \tag{3}$$

In the case where $\Omega_n(t)$ and $\mu_n(t)$ are constants, Eq. (1) produces the usual polariton dispersion relation [6]. In the absence of a shock wave, light "sees" a periodic array of polarizable elements that give rise to a band structure with both polaritonic and Bragg photonic band gaps. However, the Bragg photonic band gap for a typical crystal lattice constant (a on the order of 1 Å) is in the x-ray frequency range. In this work, we consider frequencies well below the x-ray range. In the model of Eq. (1), we consider the shock wave to be represented by a space- and time-dependent $\Omega_n(t)$ given by

$$\Omega_n(t) = \Omega_0 - \frac{1}{2}\Delta\Omega\left[\tanh\left(5\frac{na - v_st}{\beta a}\right) - 1\right], \tag{4}$$

where Ω_0 corresponds to the preshock state, $\Delta\Omega$ is the shift in Ω across the shock front, βa is the shock front thickness, and v_s is the shock speed. The factor of 5 provides scaling on β so that $\beta=1$ approximately corresponds to a shock rise distance of 1 lattice unit. An analogous relation for $\tilde{\Omega}$ provides a variation of $\mu_n(t) \equiv (\alpha/V)\tilde{\Omega}_n(t)^2$ as a function of $\Delta\tilde{\Omega}$ while α/V is taken to be constant for simplicity. In general, Ω and μ can increase or decrease under shock compression.

To determine the emission characteristics of this shocked polarizable material, we begin with a symmetry analysis of the classical equations of motion of the system. There exists a time and space translational invariance of this system that gives rise to a Bloch-like property for the fields. Radiation in physically vibrating photonic crystals has been found to possess a related property [7]. In the shocklike wave, the polarizable elements have the property that $\Omega_{n-m}(t-ma/v_s) = \Omega_n(t)$. Thus, a space and time translation operator $\hat{T}_m$ such that $\hat{T}_m f_n(t) \equiv f_{n-m}(t-ma/v_s)$ and $\hat{T}_m f(x,t) \equiv f(x-ma, t-ma/v_s)$ leaves the operators in Eq. (1) and Maxwell's equations invariant. Comparison of the fields in Eq. (1) and Maxwell's equations with and without the application of $\hat{T}_m$ leads to the result that the electric field must be of the form

$$\hat{T}_m E = E \tag{5}$$

when $\bar{P} \neq 0$ and we have taken $\hat{T}_m\tilde{\Omega}_n(t)=\tilde{\Omega}_n(t)$, and $\hat{T}_m\Omega_n(t)=\Omega_n(t)$. The magnetic and polarization fields have analogous results. The electric field is therefore of the form

$$E = \sum_k e^{ik(x-v_st)}\sum_\ell E'_{k,\ell}e^{-2\pi i\ell(v_s/a)t}, \tag{6}$$

where ℓ is an integer and k is a wave vector and H and P have similar forms. The Bloch-like property of the fields yields a condition on the radiation emitted by the shock

wave. Possible frequencies in the fields in Eq. (6) are

$$\omega' = k' v_s + 2\pi\ell \frac{v_s}{a} \tag{7}$$

where primes denote the output radiation. Possible emission frequencies into the preshock and postshock materials are those for which Eq. (7) and the dispersion relations $[\omega(k')]$ for the preshock and postshock materials have common solutions, respectively. When $\ell \neq 0$, the $2\pi\ell v_s/a$ term on the right is significantly larger in magnitude than the $k' v_s$ term since $2\pi/a \gg k'$, i.e., a is of atomic dimensions and k' corresponds to an optical or THz wave vector. Neglecting the latter term, the emission frequencies simply correspond to integral multiples of the inverse time required for the shock to propagate through a lattice unit. The $k' v_s$ term is a Doppler shift correction due to the fact that the shock front is moving. The confinement of the emitted radiation to discrete frequencies demonstrates the coherent nature of emitted radiation within this model.

A. Quantum mechanical case

In the classical case considered in the previous section, radiation is generated when the shock propagates past each lattice unit in the crystal. The total radiation from the crystal (from all lattice units) is temporally periodic, resulting in discrete emission frequencies. This section considers the case when the emission amplitude from each lattice unit is sufficiently small that only a few or no photons at all are emitted. Naively, it might seem that the temporal coherence of the emitted radiation would decrease and Eq. (7) will no longer hold. However, we will show that even in the case where a single photon is emitted from the entire crystal, that photon will be a frequency given by Eq. (7) because the shock generates a coherent quantum state of the atoms. While one might think that stimulated emission should be necessary for coherent emission in the quantum case, stimulated emission is not required when the system is coherently prepared as in, for example, so-called correlated spontaneous emission "lasers" [8].

In this section, we perform a quantum field theory analysis of a related system that yields the same emitted frequencies as the classical case, given in Eq. (7). We begin by defining a Hamiltonian that represents the shocked crystal, then find solutions of the Hamiltonian and use those for a perturbative solution to possible electromagnetic coupling. A model time-dependent Hamiltonian describing a shock is of the form

$$H = \sum_j \left(\frac{p_j^2}{2m} + \frac{1}{2} m \omega_j^2(t) (x_j - ja)^2 \right). \tag{8}$$

Here, x_j and p_j are position and momentum operators for electrons in a 1D crystal. Although explicitly time dependent, this Hamiltonian can be shown to possess time-dependent solutions with a conserved quantity. The Hamiltonian commutes with a spatiotemporal translation operator defined as

$$\hat{\tau}_m f(\{x_j\},t) \equiv f\left(\{x_j - ma\}, t - m\frac{a}{v_s} \right). \tag{9}$$

Here, $f(\{x_j\},t)$ is a function of the positions of the electrons $\{x_j\}$ and time t. The translation operator $\hat{\tau}_m$ leaves shocklike solutions invariant (to a phase) and is similar to the translation operator utilized to determine the Bloch-like properties of emitted radiation in the classical case of the previous section. The Hamiltonian commutation property implies that many-body eigenstates of $\hat{\tau}_m$ are invariant under time evolution by the Hamiltonian. Many-body eigenstates of $\hat{\tau}_m$ have the form

$$\psi_q(\{x_j\},t) = e^{iqv_s t} \prod_j \int \frac{dk_j}{2\pi} e^{ik_j(x_j - v_s t)} \sum_{n_j} \gamma_{n_j,q}(k_j) e^{-2\pi i (v_s/a) n_j t}, \tag{10}$$

where q is a quantum number, preserved in the time evolution, and the $\gamma_{n_j,q}(k_j)$ are coefficients. The form of Eq. (10) is closely related to Eq. (6). The factor of $e^{iqv_s t}$ in Eq. (10) arises in the usual Bloch fashion from the property that $\hat{\tau}_m \hat{\tau}_n = \hat{\tau}_{m+n}$. This phase factor can be expressed in other equivalent ways. The case where the preshock state of the material is the ground state is described by $q=0$.

To calculate the electromagnetic emission caused by the shock, the solutions of Eq. (10) can be used in first-order perturbation theory with the electromagnetic Hamiltonian $H' = -\Sigma_{j'}(e/mc)A(x_{j'},t)p_{j'}$ where A is the usual quantum field operator. It can be shown that this approach is valid even with the time-dependent Hamiltonian of Eq. (8). The probability of emitting a photon after the shock has propagated for a time $t \to \infty$ is

$$\left| \frac{1}{\hbar} \int_0^\infty dt \langle \psi_0;0,0,\ldots,1,\ldots,0 | H' | \psi_0;0,0,\ldots,0,\ldots,0 \rangle \right|^2, \tag{11}$$

where we consider the $q=0$ many-body state in the occupation number notation. The state $|\psi_0;0,0,\ldots,0,\ldots,0\rangle$ represents the $q=0$ state of the electrons and no photons in the system. The state $|\psi_0;0,0,\ldots,1,\ldots,0\rangle$ represents the $q=0$ state of the electrons and one photon at frequency ω'. This integral can be shown to be nonzero only for values of the emitted photon frequency ω' and wave vector k' equivalent to Eq. (7). Therefore, under the assumptions made here, any photons emitted from the shock in the quantum case are phase coherently related to each other. It might be expected that a single photon emitted from an atom in the shock wave can be emitted at any frequency. However, the shock wave "prepares" the atoms in a coherent state that collectively emits a photon only at the frequencies given by Eq. (7).

B. Scaling relations

In this section, we provide some estimates of the electric field amplitude of the coherent emission by considering scaling relations derived from simplified models of the polarization of the shocked crystal. We first consider a simple model of total surface polarization (polarization per unit area of the

shock front) $p(t) \equiv \Sigma_n P_n(t) a$ that occurs in the thick shock front limit $(2\pi v_s / \beta a \Omega \ll 1)$,

$$p(t) = P_0 a + \sum_{\ell} -\frac{a\Delta P}{2}\left[\mathrm{erf}\left(\frac{t - \ell a/v_s}{\Delta t}\right) - 1\right]. \quad (12)$$

Here, $\Delta t = \beta a / v_s$ is the time required for the shock to traverse a particular point, ΔP is the change in polarization across the shock front, and $\mathrm{erf}(z) \equiv 2/\sqrt{\pi}\int_0^z e^{-y^2} dy$. In this limit, the polarization of an element changes from the preshock to postshock equilibrium values without any oscillation at the natural frequency of each oscillator. This form is not identical to the polarization corresponding to Eq. (4), but it is more readily solved analytically. Radiation emitted from this source at frequencies $\omega = 2\pi n v_s / a$ can be shown to have electric field amplitude $E(\omega = 2\pi n v_s / a)$,

$$\left|\frac{E(\omega = 2\pi n v_s/a)}{E_{\mathrm{external}}}\right| = \left|\frac{v_s}{c}\frac{\Delta\epsilon}{2} e^{-(\pi\beta n)^2}\right|. \quad (13)$$

Here, the change in static dielectric constant is $\Delta\epsilon = 4\pi\Delta P / E_{\mathrm{external}}$. Equation (13) was obtained by utilizing the fact that the shock front thickness is of subwavelength dimensions (typically, nanometer length scale versus the 10–100 μm wavelength of emitted radiation) to determine the relationship $|E(\omega)| = (2\pi\omega/c)|p(\omega)|$.

Equation (13) predicts that the amplitude of the radiation will increase with decreasing shock front thickness, increasing dielectric change across the shock front, and increasing shock speed. The factor of v_s/c in Eq. (13) places a significant limit on the emission amplitude since this term is typically of order 10^{-5} or 10^{-4}. The amplitude is extremely sensitive to the shock front thickness, which is physically reasonable since the crystal lattice is expected to become inconsequential when the shock wave is spread out over many lattice units. The emission amplitude also drops off very rapidly with increasing harmonic number n. Equation (13) predicts that the emitted amplitude is independent of absorption γ and the resonant frequency Ω in this limit. Under experimental conditions, some dependence on these parameters may exist due to absorption of the emitted radiation as it propagates through the material toward the edge before being observed.

In a different limit, where $\beta \to 0$ and the shock changes the polarizability on a time scale faster than the natural oscillation frequency $(2\pi v_s / \beta a \Omega \gg 1)$, a classical model of the total shock front polarization $p(t)$ per area is

$$p(t) = a\Delta P \sum_m \theta\left(t - \frac{ma}{v_s}\right)\exp\left[(i\Omega' - \gamma)\left(t - \frac{ma}{v_s}\right)\right], \quad (14)$$

where $\Omega' \equiv \Omega_0 + \Delta\Omega$ and θ represents the Heaviside function. In this limit, the shock changes the equilibrium polarization sufficiently fast that resonant oscillations of each polarizable element result. It can be shown that radiation emitted from this source at frequencies $\omega = 2\pi n v_s / a$ has electric field amplitude $E(\omega = 2\pi n v_s / a)$,

$$\left|\frac{E(\omega = 2\pi n v_s/a)}{E_{\mathrm{external}}}\right| = \left|\frac{v_s}{c}\frac{\Delta\epsilon}{2}\frac{\Omega' - i\gamma}{\Omega' - i\gamma - \omega}\right|. \quad (15)$$

This amplitude of coherent emission in this case has the same limiting dependence on v_s as in Eq. (13). However, the loss factor γ plays a role and the amplitude of higher-n harmonics does not fall of as rapidly with increasing n as in the case of Eq. (13).

Note that the coherent emission frequencies of Eq. (7) do not necessarily correspond to optically active phonon modes, i.e., motion of the polarizable elements in this case does not necessarily produce radiation at the resonant frequency. However, the amplitude of Eq. (15) becomes relatively large if the coherent frequency ω is near the postshock transverse optically active Brillouin zone center phonon frequency (Ω') and the loss factor γ is relatively small. In this special case, the shock coherently excites an optically active phonon mode as it propagates.

The rise times of shock wave fronts in materials are expected to range between the limiting cases of Eqs. (13) and (15). Our molecular dynamics simulations in NaCl show some of both types of behavior depending on the shock amplitude, material temperature, and other factors. Generally, larger shock amplitudes yield sharper shock fronts and lower material temperatures yield more oscillations at the shock front.

In addition to the factors considered here, a number of other factors play a role in the amplitude of emitted coherent radiation. These include the deviation of the shock from a perfect 1D structure (i.e., a nonplanar shock wave), and thermal and other types of disordering of the crystal lattice. These effects are discussed in detail in Refs. [1,2].

III. COMPUTATIONAL EXPERIMENTS

In this section, we perform finite-difference time-domain simulations [9] of Maxwell's equations in 1D and the shocked polarization equation of motion, i.e., Eqs. (1)–(3). These simulations directly solve for the electric, magnetic, and polarization fields generated by the shock propagating through the crystal and provide qualitative insight into the factors governing the coherent radiation generation process.

For the polarization model of Eq. (1), we utilize parameters appproximately representative of a typical ionic crystal like NaCl. We set $-\bar{\Omega}_n(t)^2 \bar{P} = \mu_n(t) E_{\mathrm{external}}$ in Eq. (1) to induce some moment in the polarizable elements with a constant, uniform electric field E_{external}. Our molecular dynamics simulations of shocked NaCl yield coherent polarization oscillations in the direction of shock propagation without any applied static electric field. The 1D model employed in this work considers a static external field and polarization oscillations transverse to the propagation to enable a scalar treatment. The shock speed is taken to be $v_s = 3300$ m/s, $\Omega_0/2\pi = 4.9$ THz [6], and for a shock pressure range of 2–4 GPa we take $\Delta\Omega = 0.2 \times \Omega_0$ [10]. The lattice constant a is taken to be 4.0 Å. The absorption parameter $\gamma/\Omega = 0.29$, reasonable for ionic crystals [6]. The polarizability parameters $\tilde{\Omega}_0$, $\Delta\tilde{\Omega}$, and α/V are chosen to provide a static dielectric constant in front of the shock $\epsilon = 5.9$ and behind the

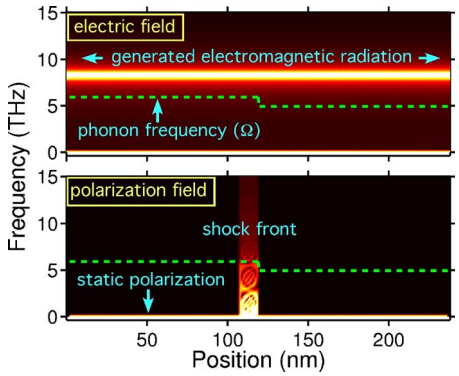

FIG. 2. (Color online) Magnitude of the Fourier transform of the electric field (top) and polarization field (bottom) for a computer simulation of the generation of coherent radiation in a model of a shocked polarizable crystal with $\Delta\epsilon=-2.4$ and $\beta=2.5$. The shock propagates to the right and induces coherent oscillations in the polarization at the shock front (bottom panel.) The polarization oscillations emit coherent radiation to the right and left (top panel.) The shock front is located around $x=120$ nm, and the resonant frequency of the polarizable dipoles (Ω) is depicted by the green dashed lines.

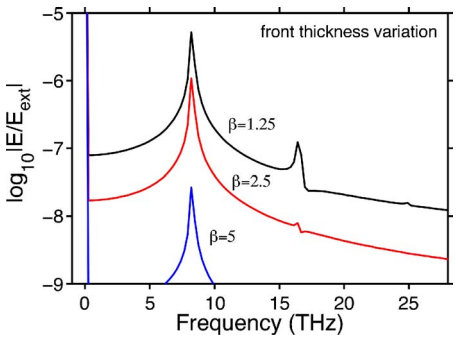

FIG. 3. (Color online) Absolute value of the Fourier transform of the electric field on the right side of the computational cell for the scenario in Fig. 2 with $\Delta\epsilon=-2.4$ and various values of β, the shock front thickness parameter. More than one discrete emission peak can be observed in the $\beta=1.25$ case. The intensity of all generated radiation peaks is weaker for thicker shock fronts.

shock $\epsilon=3.5$, modeling an approximately 4 GPa shock [11]. The static dielectric constant is given by $\epsilon=1+4\pi(\alpha/V)\times(\tilde{\Omega}/\Omega)^2$. The shock front thickness $\beta=2.5$, giving a rise distance of about 1 nm, consistent with thicknesses that are observed in molecular dynamics simulations of shock waves [1,2]. There is a short vacuum region (a few grid points) on the left and right sides of the computational cell followed by absorbing boundary conditions.

Figure 2 shows results of a FDTD simulation of the generation of radiation in the model of Eq. (1). Nonzero-frequency radiation is produced when the polarization is changed by the shock. Shown is the magnitude of the Fourier transform of the electric field E (top) and polarization field P (bottom). As the shock propagates, it changes the value of the equilibrium polarization. The resulting polarization current generates a spectrum of nonresonant polarization frequencies from zero to above 15 THz, shown in the bottom panel. The resonant frequency of the polarizable dipoles Ω is depicted by the green dashed lines in each plot. The shock front, located around $x=120$ nm, emits radiation to the left and right as it propagates to the right. The emitted radiation is narrowband despite the broad range of frequencies being excited, because the shock induces a coherent excitation of the polarization that only adds constructively at discrete frequencies, i.e., the sum over all polarizable elements has discrete frequency components but each individual polarizable element exhibits a broad range of frequency components. The frequency of the emitted radiation differs from the phonon frequencies (green dashed lines), i.e., the radiation is not produced by simple oscillations of an optically active phonon mode. The emitted radiation induces polarization waves too weak to observe on the intensity scale of the bottom panel. The polaritonic band gap in this case extends up in frequency from Ω to around 12 THz in the preshock material, but the attenuation length (on the order of 10–100 μm) is sufficiently long that no appreciable attenuation of the emitted radiation occurs during propagation to the edges of the simulated material.

The coherence time of the emitted radiation in Fig. 2 is limited by the simulation duration and can be made arbitrarily large by allowing the shock to propagate sufficiently far. Factors that limit the coherence time of the radiation include variations in the shock speed which are determined in practice by the drive mechanism of the shock wave. The observed emission frequencies are in excellent agreement with Eq. (7) since $2\pi v_s/a=8.25$ THz. While Eq. (7) predicts *possible* emission frequencies, it makes no predictions regarding the amplitude of the emitted radiation. The relative amplitudes of these frequencies are determined in part by the substructure within the periodic unit cell of the lattice. For example, we have performed molecular dynamics simulations that show that the lowest-frequency coherent polarization currents generated correspond to $\ell=2$ in Eq. (7) for a shock in the [100] direction of NaCl. In this case, the spatial length $a/2$ corresponds to the distance between atomic planes in the crystal. Therefore, some possible frequencies may be diminished or absent from the emission spectrum.

The relative simplicity of the model employed here enables the systematic study of the emission properties as a function of shock front thickness (or rise time). Figure 3 shows the absolute value of the Fourier transform of the electric field on the right side of the computational cell for the scenario in Fig. 2 with a variety of different shock front thickness parameters β. The $\beta=2.5$ case is shown in Fig. 2. More than one discrete emission frequency can be seen in the $\beta=1.25$ case. Thicker shock fronts, where the role of the crystal lattice is expressed less, provide a lower intensity of emitted radiation. While shock front thicknesses have not been experimentally measured to the level of precision of this length scale, our molecular dynamics simulations on NaCl indicate that values of β in the 2–3 range (around 1 nm) are realistic for low-amplitude elastic shock waves.

The sharp variation of emitted radiation amplitude with shock front thickness could possibly be used as a new diagnostic tool to obtain a precise measurement of the thickness of shock wave fronts, a measurement which has been challenging to make [12,13]. The predicted emitted radiation de-

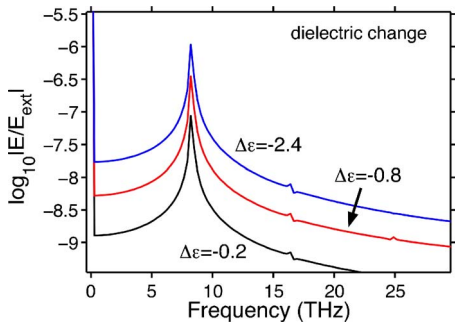

FIG. 4. (Color online) Absolute value of the Fourier transform of the electric field on the right side of the computational cell for the scenario in Fig. 2 with $\beta=2.5$ and various values of the change in the static dielectric ϵ across the shock front. Larger shifts in ϵ result in large changes in static polarization across the shock front, yielding higher emission intensities due to larger amplitudes of polarization oscillation.

pendence on β is in good agreement with Eq. (13) for $\beta=1.25$ and 2.5. Equation (13) predicts more rapid decay of emission field amplitude with β than is observed in the simulated $\beta=5$ case due to the fact that Eq. (12) represents a smoother shock front than that of Eq. (4) utilized in the simulations. Equation (15) predicts an upper bound of $|E_1/E_{\text{external}}| \approx 10^{-4.5}$ in the $\beta \to 0$ limit of the model with $v_s=3300$ m/s, consistent with the simulations of Fig. 3.

The lowest-frequency generated radiation in Fig. 3 has an electric field amplitude of about 10^{-6} times the static electric field amplitude for $\beta=2.5$. If the applied static field is 10^7 V/cm, then the emitted field amplitude is around 10 V/cm. Amplitudes computed from planar molecular dynamics simulations on NaCl (without a static applied electric field) are on the order of 0.1 V/cm [2].

We have performed simulations with a spatially linear form of Eq. (4) that yields substantially higher emission for large β ($|E/E_{\text{ext}}|=10^{-6.5}$ for $\beta=20$) than Eq. (4) with large β. This suggests the shape of the shock front plays an important role in the efficiency for large β in addition to the amount of dielectric change and front thickness. The linear form of Eq. (4) employed for these calculations has artificially sharp spectral features at the beginning and end of the linear ramp, which likely give rise to the higher emission. We expect that the smoother form given by Eq. (4) is a more realistic representation of a shock front.

Figure 4 shows the absolute value of the Fourier transform of the electric field on the right side of the computational cell for the scenario in Fig. 2 with various values of the change in the static dielectric ϵ across the shock front. Large shifts in ϵ result in large changes in static polarization across the shock front because the static polarization is given by $P=(E_{\text{external}}/4\pi)(\epsilon-1)$. Large shifts in polarization P across the shock front yield higher emission intensities due to larger polarization currents at the shock front. For the simulations in Fig. 4, $\tilde{\Omega}_0$ and $\Delta\tilde{\Omega}$ are chosen to yield $\epsilon=5.9$ in front of the shock and $\epsilon=5.9+\Delta\epsilon$ behind the shock front. The predicted emitted radiation dependence on $\Delta\epsilon$ is in good agreement with Eq. (12).

IV. CONCLUSION

We have shown that a mechanical shock wave propagating through a polarizable crystalline material can produce coherent radiation. The models employed in this work facilitate systematic study of the emission properties as functions of the shock front thickness and dielectric shift. We find that the emission amplitude is exponentially sensitive to the shock front thickness and linearly dependent on the static dielectric shift when an external electric field is applied. We have presented some simple analytical models predicting the emission amplitude. We have also shown that this classical effect has a quantum mechanical analog in the low-amplitude emission limit.

Our previous work deals with the coherent emission effect within the context of 3D molecular dynamics simulations of shock waves in NaCl. These simulations are more accurate than the simple models employed in this work but do not solve Maxwell's equations explicitly and are difficult to study in a systematic fashion. A detailed analysis of the origins of this effect, including the role of thermal disordering of the crystal, plastic deformation of the crystalline lattice, shock amplitude effects, and deviations of the shock front from perfect planarity, can be found in Ref. [1] and Ref. [2].

ACKNOWLEDGMENTS

We thank E. Ippen, F. Kaertner, and K. Nelson of MIT, J. Glownia, A. Taylor, and R. Averitt of LANL, L. Fried, D. Hicks, and N. Holmes of LLNL, and W. Nellis of Harvard University for helpful discussions. This work was supported in part by the Materials Research Science and Engineering Center program of the National Science Foundation under Grant No. DMR-9400334. This work was performed in part under the auspices of the U.S. Department of Energy by University of California, Lawrence Livermore National Laboratory under Contract No. W-7405-Eng-48.

[1] E. J. Reed, M. Soljačić, R. Gee, and J. D. Joannopoulos, Phys. Rev. Lett. **96**, 013904 (2006).
[2] E. J. Reed, M. Soljacic, R. Gee, and J. D. Joannopoulos (unpublished).
[3] G. E. Hauver, J. Appl. Phys. **36**, 2113 (1965).
[4] R. K. Linde, W. J. Muri, and D. G. Doran, J. Appl. Phys. **37**, 2527 (1966).
[5] P. Harris and H. Presles, J. Chem. Phys. **77**, 5157 (1982).
[6] C. Kittel, *Introduction to Solid State Physics* (John Wiley and Sons, New York, 1996).
[7] M. Skorobogatiy and J. D. Joannopoulos, Phys. Rev. B **61**, 15554 (2000).
[8] M. O. Scully and M. S. Zubairy, *Quantum Optics* (Cambridge University Press, Cambridge, U.K., 1997).

[9] A. Taflove and S. C. Hagness, *Computational Electrodynamics: The Finite-Difference Time-Domain Method* (Artech House, Norwood, MA, 2000).
[10] A. M. Hofmeister, Phys. Rev. B **56**, 5835 (1997).
[11] R. A. Bartels and P. A. Smith, Phys. Rev. B **7**, 3885 (1973).
[12] K. T. Gahagan, D. S. Moore, D. J. Funk, R. L. Rabie, S. J. Buelow, and J. W. Nicholson, Phys. Rev. Lett. **85**, 3205 (2000).
[13] O. L. Muskens, A. V. Akimov, and J. I. Dijkhuis, Phys. Rev. Lett. **92**, 035503 (2004).